Laser and Particle Beams (2001), *19*, 59–65. Printed in the USA.

Effects of self-generated electric and magnetic fields in laser-generated fast electron propagation in solid materials: Electric inhibition and beam pinching

A. BERNARDINELLO,[1] D. BATANI,[1] A. ANTONICCI,[1] F. PISANI,[1] M. KOENIG,[2] L. GREMILLET,[2] F. AMIRANOFF,[2] S. BATON,[2] E. MARTINOLLI,[2] C. ROUSSEAUX,[3] T.A. HALL,[4] P. NORREYS,[5] AND A. DJAOUI[5]

[1]Dipartimento di Fisica "G. Occhialini" and INFM, Università degli Studi di Milano Bicocca, Piazza della Scienza, 3, 20126 Milano, Italy
[2]LULI, UMR n.7605, CNRS–CEA–X–Paris VI, Ecole Polytechnique, 91128 Palaiseau, France
[3]Commisariat à l'Energie Atomique, 91680 Bruyères-le Châtel, France
[4]University of Essex, Wivenhoe Park, Colchester CO4 35Q, United Kingdom
[5]Central Laser Facility, Rutherford Appleton Laboratory, Chilton, Didcot, OX11 0QX, United Kingdom

(RECEIVED 30 November 2000; ACCEPTED 5 February 2001)

Abstract

We present some experimental results which demonstrate the presence of electric inhibition in the propagation of relativistic electrons generated by intense laser pulses, depending on target conductivity. The use of transparent targets and shadowgraphic techniques has made it possible to evidence electron jets moving at the speed of light, an indication of the presence of self-generated strong magnetic fields.

1. INTRODUCTION

Fast electron generation in laser–plasma interaction is an important subject (Forslund *et al.*, 1977; Hares *et al.*, 1979; Rosen *et al.*, 1979; Harrach & Kidder, 1981; Bond *et al.*, 1982; Luther Davies *et al.*, 1987; Rousse *et al.*, 1994; Malka & Miquel, 1996) recently rediscovered thanks to developments in short-pulse high-energy laser technology, and especially to the "fast ignitor" approach to inertial confinement fusion (Tabak *et al.*, 1994; Atzeni, 1995). This scheme is based on decoupling the two phases of compression and ignition of the nuclear fuel. In the last phase, a high-intensity short-pulse laser generates relativistic electrons which should propagate through the compressed capsule and lose their energy, heating the DT fuel and starting its ignition.

Key aspects to assess the feasibility of fast ignition are the characterization of the fast electron source (temperature flux, and the opening angle of the electron beam) and of the energy deposition of fast electrons in matter.

Theoretically the last problem has been studied by Deutsch *et al.* (1996) using a collisional model based on the stopping power formulas developed by Val'chuk *et al.* (1995). In this context, a first experiment (Hall *et al.*, 1998) has been realized with the VULCAN laser system at the Rutherford Appleton Laboratory, to measure fast electron propagation in laser-shock-compressed matter.

Another important aspect influencing fast electron propagation has recently been much discussed in literature (Bell *et al.*, 1997; Davies *et al.*, 1997; Bernardinello *et al.*, 1999; Batani *et al.*, 2000), namely, the so called electric inhibition: The huge electric fields generated as the fast electrons penetrate into the target can prevent any further penetration, unless the free background electrons in the material set up a current which neutralizes such electric fields. These effects are predicted to play a fundamental role, depending on material conductivity, and even to be the major limiting factor in fast electron propagation.

In the present experiment, performed at the LULI TW laser chain, we compared fast electrons propagation in materials with different electrical properties. To study the dynamics of the propagation of the fast electrons inside the targets, we used transparent glass targets and a short-pulse probe beam perpendicular to the interaction beam, which allowed a picture of the target to be recorded on a CCD camera. As the electrons propagate inside the target, they ionize the material, which becomes opaque to the probe. By varying the delay between the interaction and the probe beam, we performed a time-resolved shadowgraphy, so that

Address correspondence and reprint requests to: Andrea Bernardinello, Dipartimento di Fisica "G. Occhialini" and INFM, Università degli Studi di Milano-Bicocca, Piazza della Scienza, 3-20126 Milano, Italy. E-mail: andrea.bernardinello@mib.infn.it.

we could follow the evolution of the ionized region inside the target.

2. EXPERIMENTAL SETUP

The principle of the experiment is illustrated in Figure 1. K_α emission spectroscopy was used as diagnostic for the propagation of electrons. The high flux laser, with a pulse duration of 350 fs and a contrast ratio of about 10^8, is perpendicularly focused on the target placed at the center of a vacuum chamber. The fast electrons are accelerated in the zone of interaction between the laser and the target, and propagate through a first layer of variable thickness ("propagation layer"), alternatively made of materials with differing electrical properties (plastic or aluminum). After this, the fast electrons reach two layers of fixed thickness of fluorescent materials (20 μm of Mo and 20 μm of Pd) where they induce K_α emission, depending on their residual energy. By varying the thickness of the propagation layer from shot to shot, we could measure the typical penetration range of the fast electrons in the given material. K_α photons are detected by a CCD camera placed outside the interaction chamber, facing the rear side of the target, and used in single hit mode to allow spectroscopic analysis. A fourth 50-μm plastic layer on the rear side of the target prevented the electrons coming directly from the interaction zone and moving around the target to hit the fluorescent layer, inducing a spurious K_α emission.

To assure the same interaction conditions in the case of plastic targets, a first layer of 1.5 μm Al was added. Hence, any difference in experimental K_α yield was due only to differences in electron propagation through the solid materials, and not to a different conversion rate or temperature of the produced fast electrons.

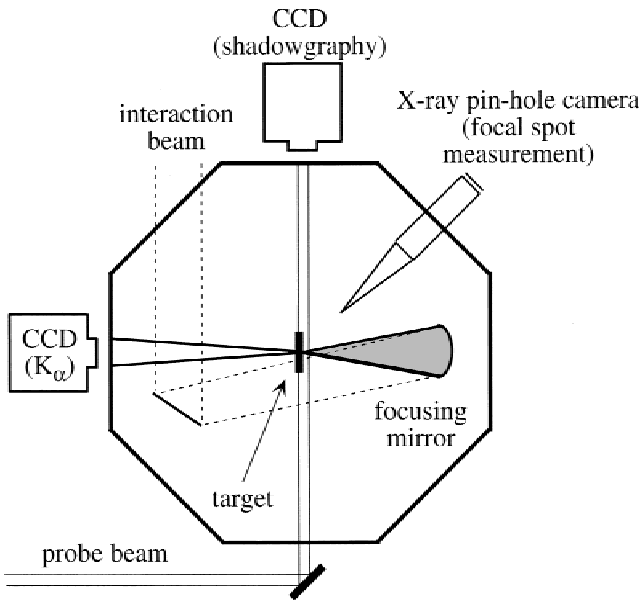

Fig. 1. Principle of the experiment.

For shadowgraphy we used glass targets with an aluminum coating 10 μm thick to avoid direct ionization from the main laser beam. Perpendicular to this, a short pulse probe beam was shot with a time delay which could be varied using a delay line. The probe beam consisted of a small fraction of the nonconverted main beam (its wavelength was therefore $\lambda = 1.057$ μm). An X-ray pinhole camera (with a resolution of 7 μm) was employed to image the shape of the focal spot.

3. THE EXPERIMENT ON ELECTRIC INHIBITION

We realized two series of shots in which the laser intensity on target was changed by varying the focusing conditions. In the first one, the focal spot diameter was $\approx$30 μm and the intensity was 1–2 $\times$ 10^{18} W/cm^2, while in the second one, the spot was $\leq$10 μm and the intensity 1–2 $\times$ 10^{19} W/cm^2. Plastic (polyethylene) had a thickness between 50 and 175 μm, while aluminum was 6 to 37 μm thick in the low intensity case; at higher intensities they were, respectively, 50 to 400 μm and 11.5 to 300 μm to match the predicted increased penetration.

Figure 2 shows the ratio of K_α yield of palladium and molybdenum versus the thickness of the material crossed by the electrons; it refers to aluminum targets and a laser intensity of $\approx$1–2 10^{19} W/cm^2. The results have been compared with numerical simulations made for different temperatures with the PROPEL Monte Carlo propagation code, which calculates the energy loss and the angular scattering of the fast electrons as due to collisions with the target electrons and ions (Schlegel *et al.*, 1999). K_α yield is calculated taking into account the target self-absorption. The Monte Carlo simulations reproduce the experimental results, within the limits of the error bars, using temperatures $\approx$400–500 keV. This temperature is consistent with the scaling law by Beg *et al.* (1997) for resonant absorption, even if, due to our large experimental error bars, we cannot speak of a precise agreement or exclude other scaling laws (Glinsky, 1995). In the low intensity case we found $T = 170$–200 keV.

Figure 3 shows the experimental Mo K_α emission as a function of the propagation layer thickness for both plastic and aluminum targets at intensities of 1–2 $\times$ 10^{19} W/cm^2. The curves are exponential fits to the results, that is, $\exp(-R/R_0)$, and give a typical value for the experimental penetration of $R_0 \approx 230 \pm 40$ μm for Al and 180 ± 15 μm for CH. The large error bars are due to the big fluctuations from shot to shot in laser energy, duration, and focalization, but also, we think, to the very nonlinear aspect of the interaction at such high laser intensities. Figure 3 also shows a similar interpolation of numerical results for an electron temperature of 400 keV. The numerical value for Al ($R_0 = 235 \pm 10$ μm) is compatible with the experimental result. Here the error range on the numerical values are obtained by considering the typical shot-to-shot fluctuations in laser pulse and

https://doi.org/10.1017/S0263034601191093 Published online by Cambridge University Press

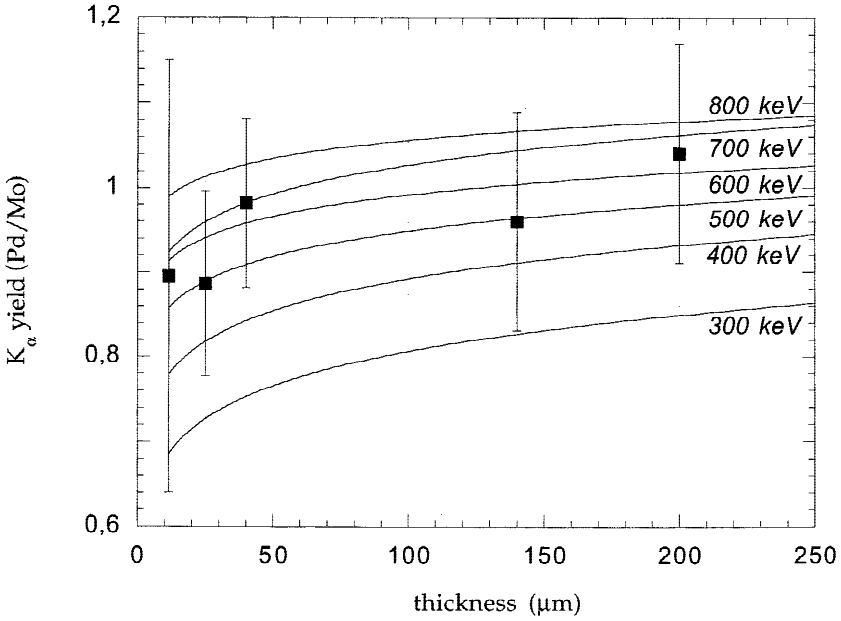

Fig. 2. Experimental (squares) and numerical (lines only, no symbols) ratio of Pd and Mo K_α yield.

how they influence the electron temperature and the propagation range.

In the case of plastic, there is instead a large discrepancy, the numerical predictions being 690 ± 20 μm. Therefore, while fast electron propagation in Al can fairly well be described by a purely collisional model, a strong inhibition of penetration is evident in plastic targets.

To understand our results, one must take into account the effects of the very high electric fields generated by space charge separation, as the fast electrons are accelerated inside the target. These will strongly inhibit the propagation of fast electrons unless neutralized by a return current in the target. Therefore, the response of the target strongly depends on material conductivity.

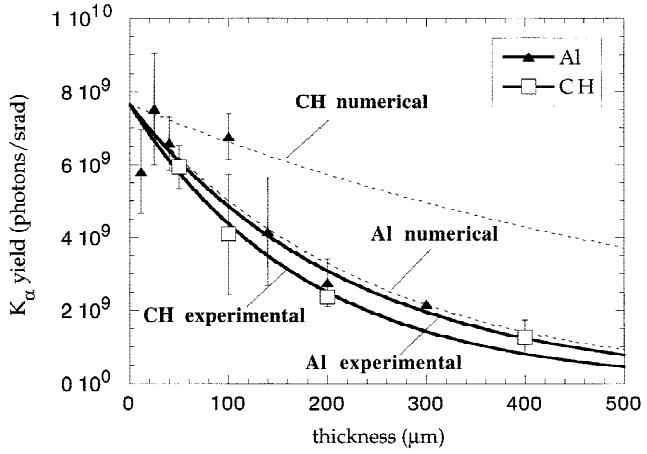

Fig. 3. Experimental and numerical results for Mo K_α yield versus target thickness at $I_L = 1\text{–}2 \times 10^{19}$ W/cm^2. The lines are exponential interpolations of data. Error bars on experimental points are given by the standard deviation of results. Where there are no error bars, a single experimental point has been obtained at the corresponding thickness.

Following the model by Bell *et al.* (1997), the typical penetration range, z_0, due to electric fields alone is proportional to the conductivity:

$$z_0\,(\mu\text{m}) = 3{\cdot}10^{-3}\,\sigma_6 T_h^2\,(fI_{17})^{-1}, \qquad (1)$$

where σ_6 is the conductivity in units 10^6 $(\Omega\text{m})^{-1}$, T_h is the temperature of the fast electrons in kiloelectron volts, I_{17} is the laser intensity on target in units 10^{17} W/cm^2, and f is the fraction of the laser energy converted into fast electrons.

The main aspects which distinguish electric and collisional effects are that the first are proportional to target thickness, while the latter are proportional to areal density. Hence the use of targets of different densities (and electrical properties) appears to be a good way to test electric versus collisional effects on fast electron propagation.

Our Al results imply that $z_0 \gg R_{coll}$ which is indeed found by inserting our typical experimental parameters in the formula for z_0 and by considering the Al room temperature conductivity ($\sigma_0 = 2.7\ 10^7\ (\Omega\text{m})^{-1}$). An additional problem is that the target itself is heated by the passage of the fast electrons, which deposit their energy. In a very simple calculation, by considering the volume crossed by fast electrons and a mean energy deposition (Hubbel & Birkoff, 1982), it is possible to evaluate an average Al temperature of the order of a couple of electronvolts due to such an effect. The conductivity of Al as a function of temperature can be calculated by using the results by Milchberg *et al.* (1988), or the models presented in Benuzzi *et al.* (1998). In this temperature range, it decreases due to quantum-mechanical effects, although the obtained conductivity values are still compatible with our results.

The situation is more complex in the case of CH targets. The conductivity of cold plastic ($\sigma = 10^{-11}$ $(\Omega\text{m})^{-1}$) in Eq. (1) gives a nonrealistic penetration less than 1 μm.

https://doi.org/10.1017/S0263034601191093 Published online by Cambridge University Press

Hence a phase transition from insulator to conductor which produces free electrons available for the neutralizing return current is essential to explain penetration. This is due both to heating of the target induced by fast electrons and to electric breakdown of plastic. The average temperature reached in plastic must be of the same order as in Al (we have roughly the same experimental penetration). Although no models or measurements allow calculation of the electric conductivity for plastic at the temperatures in which we are interested, we can infer that electric field effects will remain more important in the case of CH. Especially, one must consider that heating will have opposite effects on Al and CH conductivity: the first one is reduced with time (but keeping quite high values), while the second one increases starting practically from zero.

Figure 4 shows the experimental Mo K_α yields versus thickness for the lower laser intensity case ($1–2 \times 10^{18}$ W/cm^2). In this case, the numerical predictions are 70 ± 10 μm for Al and 350 ± 5 μm for CH for a temperature of 175 keV, while the experimental results are 60 ± 20 μm and 220 ± 50 μm, respectively.

Again, we see that collisional numerical results for Al are in agreement with experimental ones, within the error bars, while for CH the disagreement is much larger. With respect to the high intensity case, one can observe that the experimental penetration in plastic is not shorter, but about the same as with the high intensity shots, if not increased. This is in agreement with the prediction of Eq. (1). The seeming paradox of a lower penetration at higher electron temperature can only be explained with electric inhibition. Also, despite the large error bars, a purely collisional explanation must be ruled out in plastic, since it would imply a nonrealistically low fast electron temperature of ≈90 keV in the low intensity case, and an even lower temperature of ≈75 keV in the high intensity case. These would be in complete disagreement with Al results (the temperature must be the same!), and with published scaling laws (Beg, 1997; Glinsky, 1995).

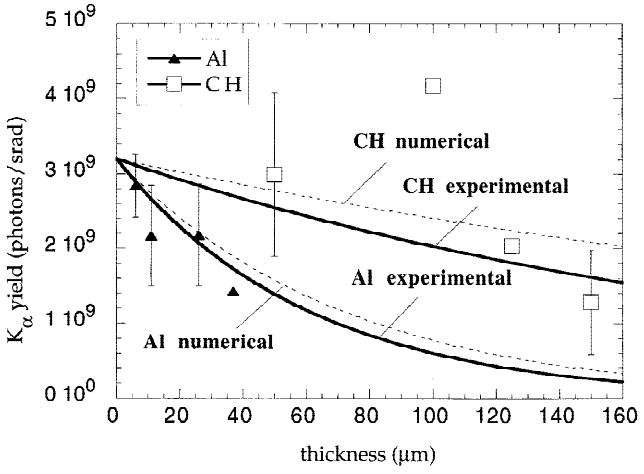

Fig. 4. Experimental and numerical results for Mo K_α yield at $I_L = 1–2 \times 10^{18}$ W/cm^2. Lines and error bars as in Figure 3.

It is also possible to use the results shown in Figures 3 and 4 for Al to obtain the efficiency of energy conversion from laser to fast electrons. To do this, the experimental K_α yield must be corrected by considering the CCD collection solid angle, the transmittivity to X rays of the windows before the CCD and the target self-absorption of K_α photons. In this way we could match the experimental values to those predicted by the code (as already done in Figures 3 and 4) and by assuming a conversion factor $f = 15\%$ at $I_L = 1–2 \times 10^{18}$ W/cm^2 and $f \approx 25\%$ at $I_L = 1–2 \times 10^{19}$ W/cm^2. We also assumed that only 50% of the laser pulse energy was contained inside the focal spot (this is a reasonable assumption for these kinds of lasers, also made by other authors (e.g., Beg, 1997)). So there is a nonnegligible increase in the conversion efficiency with increasing laser intensity. Once more, this implies a stronger inhibition of fast electrons in CH; in fact in Eq. (1), the range is inversely proportional to the conversion factor.

Let us note explicitly that the conversion efficiency and fast electron temperature cannot be obtained from CH results, which are not described by the collisional code. This is why we only considered the Al results in Figure 2.

As a final remark, we observe that the results obtained by Davies *et al.* (1997) using his Fokker–Planck code, which includes both collisions and self-generated electric and magnetic fields, and in which the heating induced by the passage of the fast electrons inside the targets is calculated self-consistently, agree fairly well with the experimental ones, therefore confirming the role of the electric field due to charge separation (Pisani *et al.*, 2000).

4. THE SHADOWGRAPHIC EXPERIMENT

The results obtained with transparent targets and the probe beam are shown in Figures 5 and 6 for the low and high intensity cases, respectively. In both cases we show a sequence of three images taken with different time delays between the two beams. The time resolution was ≈400 fs, while space resolution was ≈5 μm.

The images show an isotropic expanding ionization cloud, but also thin jets propagating at higher speed, produced in the laser focal spot region. From the delay between the interaction and the probe beam and the extension of the cloud and the jets it was possible to calculate their speeds. We found that the jets are moving close to the velocity of light, while the ionization clouds are somewhat slower, even if their speed is a large fraction of c (about $\frac{1}{2}$ in the high intensity case).

In principle, the ionization can be due not only to fast electrons, but also to X rays produced in the interaction. Hence, we used a slightly modified target, in order to discriminate between these two factors: A further layer of aluminum (10 μm thick) was placed before the target, separated from this by an ≈200-μm-thick vacuum gap. In Figure 7 we show two images taken with the same time delay (6 ps) between the interaction and the probe beam. While in the

https://doi.org/10.1017/S0263034601191093 Published online by Cambridge University Press

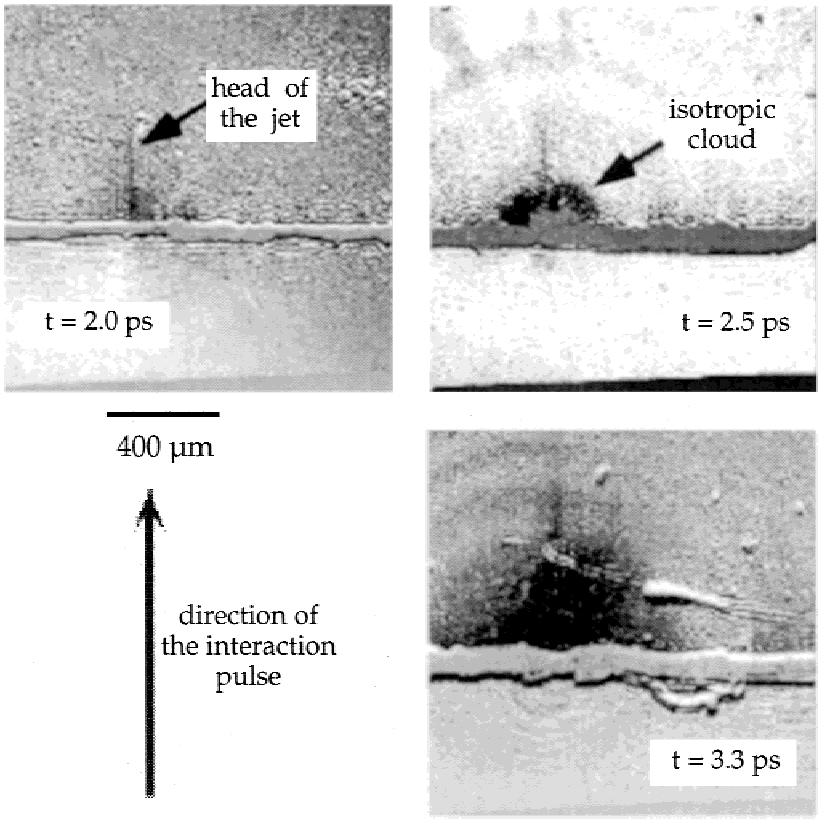

Fig. 5. Three images obtained with the shadowgraphy technique (low intensity: $I_L = 10^{18}$ W/cm^2).

case of "normal" targets (Fig. 7a), a large and well-developed cloud can be observed, in the case of modified targets (Fig. 7b), no ionization could be recorded. This excludes the possibility that the ionization pattern is due to X rays, as these would cross the vacuum layer. Instead, the lack of ionization in Figure 7b can be easily explained if it is due to fast electrons, as they cannot cross vacuum due to the onset of a strong electric field on the back side of the first aluminum layer as they start escaping from the surface. Figures 5 and 6 not only show the presence of the jets, but also that their propagation is stable on macroscopic distances ($\approx$1 μm). The presence of the relativistic electron jets obviously points out the role of the strong self-generated magnetic fields and their pinching effects.

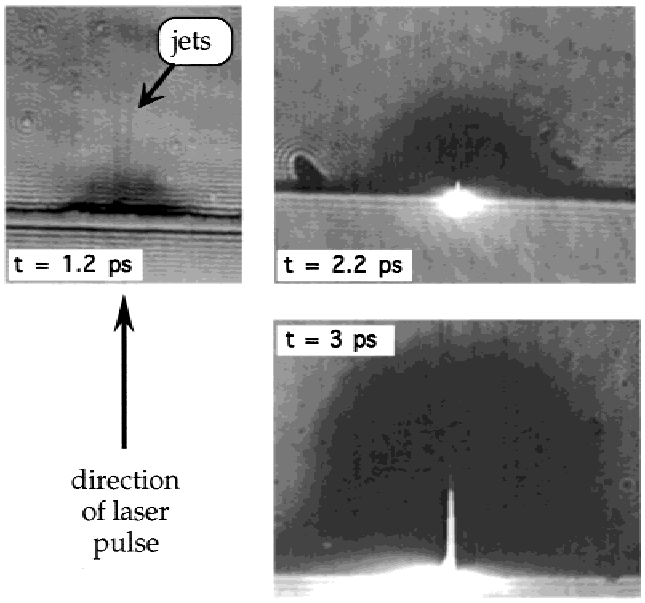

Fig. 6. Three images obtained at high intensity ($I_L = 10^{19}$ W/cm^2).

The magnetic field strength can be obtained, for instance, using the formula (Davies *et al.*, 1997)

$$B\,(\mathrm{MG}) = 76.6\sigma_6^{-1}\tau R^{-1} f I_{17}^{2/3}\lambda^{-2/3}, \qquad (2)$$

where again we have the problem of estimating the value of conductivity in the hot plastic target (τ is the pulse duration in picoseconds, R the focal spot radius in microns and λ is the laser wavelength in microns). If we use Bell *et al.*'s (1997) formula (1) and the experimental value of penetration at high intensity ($z_0 = 180$ μm), we find $\sigma_6 \approx 4$. This must be considered as an effective value (in reality σ changes in space and time inside the target). Even if this conductivity is still one order of magnitude lower than that of Al at room temperature, yet it is comparable to that of Al at temperatures of a few electronvolts. When we use this value in Eq. (2), we get $B \approx 6$ Mgauss.

https://doi.org/10.1017/S0263034601191093 Published online by Cambridge University Press

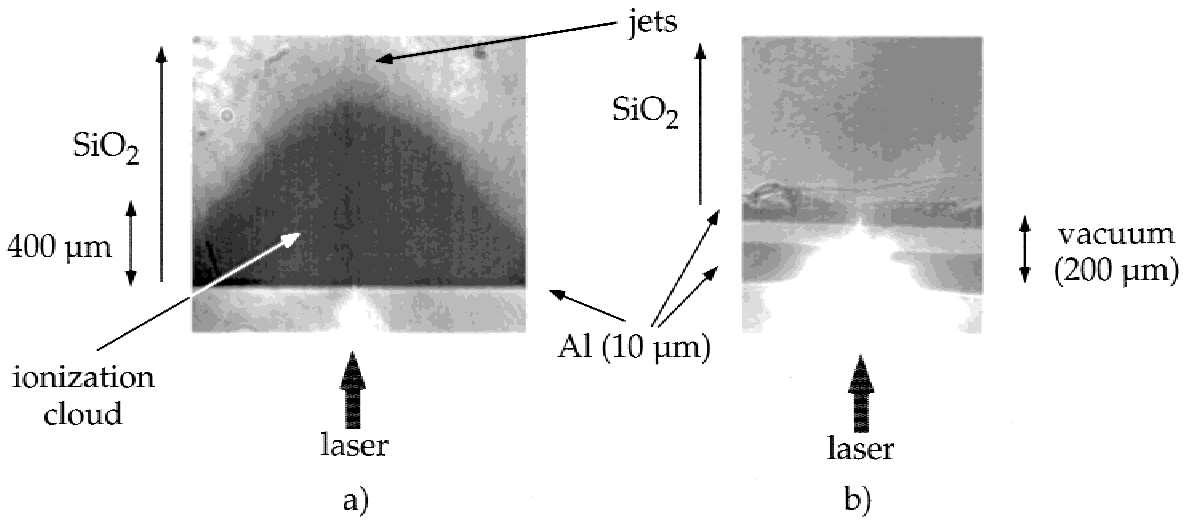

Fig. 7. Comparison between two images obtained with the same time delay (6 ps) after laser-target interaction with a normal target (a) and with an extra Al layer in front of it (b). In the latter case, no ionization is detected in the glass.

For comparison let us observe that the value of the fast electron current is $I_{hot} \approx \eta E_L e/(T_{hot}\tau) \approx 40$ MA. The corresponding current density is $J_{hot} = I_{hot}/\pi R^2 \approx 1.3 \times 10^{13}$ A/cm^2. Using Biot and Savart's law, we would find an incredibly high value of the magnetic field (at the beam edge): $B = 8$ Ggauss. The difference between the two values of B is obviously related to the presence of the return currents (which appear in Eq. (2) through the conductivity of the material). Another limit to be considered is that the maximum current which can be carried by an electron beam (in vacuum) is given by the Alfvén limit I_A (A) = 17,000 $\beta\gamma \approx 0.03$ MA, which implies $B \approx 6$ Mgauss. In a material, which really counts is the total current $I = I_{fast} - I_{return}$. Hence, at the moment, we can speculate that either the jets carry a current equal to the Alfvén limit (i.e., they contain about 1:10^3 of the fast electrons), or there is a return current inside the jets, so that the total net current is again of the order of the Alfvén value.

Apart from the role of magnetic beam pinching, other effects may be connected to electron propagation and may explain jet formation. In particular, the presence of hot spots in the laser focal spot (Fig. 8) can lead to the creation of localized populations of electrons characterized by higher energies. Another mechanism can be the so-called electrothermal instability (Haines, 1981): At the beginning, the ionization effectively is zero, due to the nature of the target (glass, i.e., an insulator), and the electrons cannot penetrate into the target. However, where there is any penetration, the material is heated and ionized. This makes penetration possible inside these regions, which are therefore crossed by a higher current and further heated and ionized, allowing a locally higher returned current and increased penetration. This is, of course, an unstable mechanism, which in the end, creates low resistivity channels where fast electrons propagate (and around which strong magnetic fields develop).

5. CONCLUSIONS

In conclusion, we have given the experimental evidence of electric inhibition and of relativistic jets of electrons in fast-ignitor related experiments.

In conductors, the larger number of background electrons can neutralize the electric field in an effective way, and the electric effects can be considered, in first approximation, negligible, while in insulators, the electric response of matter is less important, which leads to an inhibition in the propagation and to an effective penetration shorter than that predicted with collisional models. In any case, a proper analysis of the results of the propagation of electrons must take into account both collisions and electric effects.

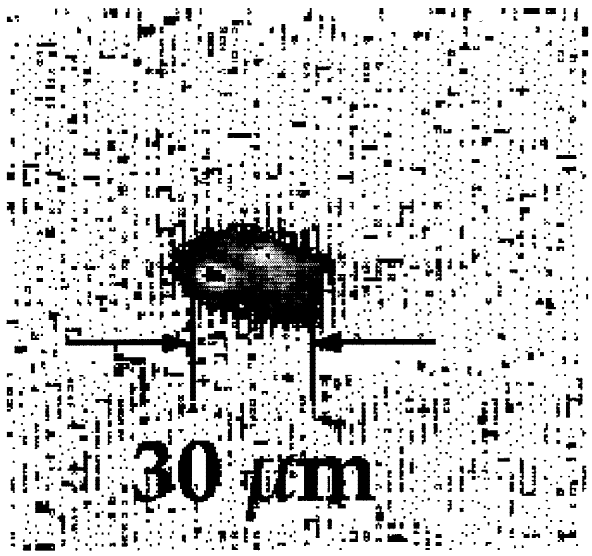

Fig. 8. Image of the laser focal spot taken with a pinhole camera showing regions of higher irradiance (low intensity case).

https://doi.org/10.1017/S0263034601191093 Published online by Cambridge University Press

Shadowgraphic images of transparent targets show the presence of a collimated jet propagating at the speed of light on macroscopic distances, therefore revealing the presence of self-induced strong magnetic fields. Though we did not perform any measurement, we can infer an upper limit for B to be a few megagauss, again implying the presence of a strong return current in order to explain the observed propagation (which appears to be stable for about 1 mm).

Finally, targets with a vacuum gap show that in vacuum, where breakdown cannot take place, no propagation of the fast electrons is possible.

ACKNOWLEDGMENTS

This work has been supported by the TMR European Program, contract n. ERBFMGECT950044.

REFERENCES

Atzeni, S. (1995). *Jpn. J. Appl. Phys.* **34**, 1980.
Batani, D. *et al.* (2000). *Phys. Rev. E* **61**(5), 5725.
Beg, F.N. *et al.* (1997). *Phys. Plasmas* **4**, 447.
Bell, A.R. *et al.* (1997). *Plasma Phys. Contr. Fus.* **39**, 653.
Benuzzi, A. *et al.* (1998). *Phys. Plasmas* **5**(6), 2410.
Bernardinello, A. *et al.* (1999). *Laser Part. Beams* **17**(3), 519.
Bond, D.J., *et al.* (1982). *Plasma Phys.* **24**, 91.
Davies, J. *et al.* (1997). *Phys. Rev. E* **56**, 7193.
Deutsch, C. *et al.* (1996). *Phys. Rev. Lett.* **77**, 2483.
Forslund, D.W. *et al.* (1977). *Phys. Rev. Lett.* **39**, 284.
Glinsky, M.E. (1995). *Plasma Phys.* **2**, 2796.
Haines, M.G. (1981). *Phys. Rev. Lett.* **47**, 917.
Hall, T.A. *et al.* (1998). *Phys. Rev. Lett.* **81**, 1003.
Hares, J.D. *et al.* (1979). *Phys. Rev. Lett.* **42**, 1216.
Harrach, R.J. & Kidder, R.E. (1981). *Phys. Rev. A* **23**, 887.
Hubbel, H.H. Jr. & Birkoff, R.D. (1982). *Phys. Rev. A* **26**, 2460.
Luther Davies, B. *et al.* (1987). *Phys. Rev. A* **35**, 4306.
Malka, G. & Miquel, J.L. (1996). *Phys. Rev. Lett.* **77**, 75.
Milchberg, H.M. *et al.* (1988). *Phys. Rev. Lett.* **61**, 2364.
Pisani, F. *et al.* (2000). *Phys. Rev. E* **62**, R5927.
Rosen, M.D. *et al.* (1979). *Phys. Fluids* **22**, 2020.
Rousse, A. *et al.* (1994). *Phys. Rev. E* **50**, 2200.
Schlegel, Th. *et al.* (1999). *Phys. Rev. E* **60**, 2209.
Tabak, M. *et al.* (1994). *Phys. Plasmas* **1**, 1626.
Val'chuk, V.V. *et al.* (1995). *Plasma Phys. Rep.* **21**, 159.